On the use of skin texture features for gender recognition: an experimental evaluation

Francesco Bianconi[1], Fabrizio Smeraldi[2,1], Maryam Abdollahyan[2], and Perry Xiao[3]

[1]Department of Engineering, Università degli Studi di Perugia
93 Via G. Duranti, 06125 Perugia, Italy
Email: {bianco}@ieee.org

[2]Centre for Intelligent Sensing, Queen Mary University of London
Mile End Road, London E1 4NS, United Kingdom
Email: {f.smeraldi, m.abdollahyan}@qmul.ac.uk

[3]School of Engineering, London South Bank University
103 Borough Road, London SE1 0AA, United Kingdom
Email: {perry.xiao}@lsbu.ac.uk

***Abstract*— Skin appearance is almost universally the object of gender–related expectations and stereotypes. This notwithstanding, remarkably little work has been done on establishing quantitatively whether skin texture can be used for gender discrimination. We present a detailed analysis of the skin texture of 43 subjects based on two complementary imaging modalities afforded by a visible-light dermoscope and the recently developed Epsilon sensor for capacitive imaging. We consider an array of established texture features in combination with two supervised classification techniques (1-NN and SVM) and a state-of-the-art unsupervised approach (t-SNE). A statistical analysis of the results suggests that skin microtexture carries very little information on gender.**

***Keywords*— Gender recognition, Skin, Texture, SVM**

I. Introduction

The ability to distinguish between male and female is essential to the survival of the species, and it is therefore hardly surprising that nature has provided plenty of visual cues through which genders can be effectively discriminated. These vary from secondary sexual characteristics to subtler behavioural cues such as, for instance, gait. Accordingly, some of the main visual biometric technologies originally developed for person identification have proved able to discriminate between genders, often with little or no modification. Gender recognition can for instance be performed using low frequency information from the contour of the face [6], [15], [20]. Likewise, kinematic data from gait analysis [1], [26], [14] can be used to discriminate between men and women.

To the best of our knowledge, however, very little work has been done on the gender discrimination potential of another established visual biometric modality, namely skin texture. This is even more remarkable because the perception of skin is heavily sexualised in the media and in society. For example, skin care products are marketed differentially to both sexes with a heavy emphasis on appearance. In some cultures, expectations on skin appearance may push women to avoid exposure to the sun or use skin–lightening products [9] in order to achieve a lighter skin tone associated with refinement and high social status. Conversely, where a premium is placed on a tanned appearance that implies health, women (and men) may resort to indoor tanning [7].

Gender differences in skin appearance therefore partake of the biological trait [8] and of the acquired social construct. The question of whether such differences allow discriminating between the sexes arguably has a sociological interest, besides its computational relevance. This appears to create a feedback loop where stereotypes and expectations on skin appearance reinforce social behaviour that in turn leads to the preservation, acquisition or enhancement of the desired appearance.

In this work, we investigate a quantitative approach to gender recognition based on skin microtexture. We consider two different imaging modalities, namely optical imaging with a professional dermoscope and capacitive imaging with the novel Epsilon sensor described in Section II. Skin texture was acquired from the back of the hand and the palm (that are known to be useful for identity recognition), as well as from the inner forearm of 43 subjects. We considered a variety of texture descriptors of known effectiveness, namely auto-correlation, Gabor filters, local binary patterns, co-occurrence features, granulometric analysis and the semi-variogram. To the resulting feature vectors we applied both supervised classification (1-NN, SVM) and a state-of-the-art unsupervised dimensionality-reduction technique (t-SNE [23]); we then performed a statistical analysis of the significance of classification results using Fisher's exact test. Rather surprisingly, although our results confirmed that skin texture information, as previously documented, provides very useful clues for person identification, no gender classification is feasible, inter-subject variability swamping the difference between the two

Sub. ID# (gender)	BH	FR	PL
#6 (male)	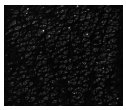	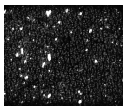	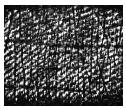
#9 (female)	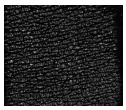	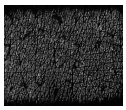	

Fig. 1. Sample images acquired with the capacitive device (Epsilon). The approximate scale (length on paper / length on inspected area) is 1:1.

Sub. ID# (gender)	BH	FR	PL
#6 (male)	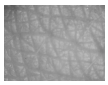	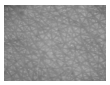	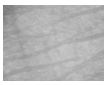
#9 (female)	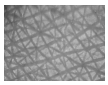	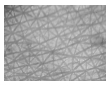	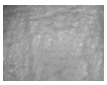

Fig. 2. Sample images acquired with the digital dermoscope (Proscope). The approximate scale (length on paper / length on inspected area) is 3:1.

sexes. Notably, our findings are markedly different from those available in the literature [25]: we argue quantitatively that if one controls for identity, very little can be inferred from skin texture about gender.

II. Dataset and acquisition

Sample images of skin were acquired from a population of 43 subjects (24 males, 19 females), average age 32.1 $\pm$ 14.2. The ethnic stratification [16] of the sample was as follows: White (27), Asian / Asian British (7), Black / African / Caribbean / Black British (7) and Mixed / multiple ethnic groups (2). The acquisition process was performed using two different devices: a digital optical dermoscope [5] (ProScope HR2, Bodelin Technologies, United States) and a capacitive fingerprint sensor (Epsilon, Biox Systems Ltd, United Kingdom – for details see Refs. [18], [4]). From each of the back of the hand (BH), forearm (FR) and palm (PL) of the upper left limb of each of the participants four images were acquired using both devices (Epsilon and Proscope). Images of the inspected parts were taken in different areas and with no predefined position or relative orientation between the devices and the skin. Sample images acquired with both systems are shown in Figs. 1–2.

III. Feature extraction

The following six texture descriptors were considered in this study: 1) autocorrelation, 2) Gabor filters, 3) grey-level co-occurrence matrices (GLCM), 4) local binary patterns (LBP), 5) granulometry and 6) semi-variogram. The basics of each method are recalled here below.

A. Autocorrelation

Autocorrelation is an estimator of the self-similarity of an image at different distances. For a given image $\mathbf{I}$ the autocorrelation under a vertical shift δx and a horizontal shift δy can be defined as follows [19]:

$$r = \frac{1}{\sqrt{\sum_{w=1}^{W}\sum_{h=1}^{H}\left[\mathbf{I}_{\delta x,\delta y}(h,w) - \bar{\mathbf{I}}_{\delta x,\delta y}\right]^2}} \cdot \cdot \frac{\sum_{w=1}^{W}\sum_{h=1}^{H}\left[\mathbf{I}_{\delta x,\delta y}(h,w) - \bar{\mathbf{I}}_{\delta x,\delta y}\right]\left[\mathbf{I}(h,w) - \bar{\mathbf{I}}\right]}{\sqrt{\sum_{w=1}^{W}\sum_{h=1}^{H}\left[\mathbf{I}(h,w) - \bar{\mathbf{I}}\right]^2}} \quad (1)$$

where $\bar{\mathbf{I}}$ indicates the mean value of $\mathbf{I}$, and H, W respectively the vertical and horizontal dimensions of the image. In order to obtain rotation-invariant features we averaged the correlation coefficient r over eight angularly equispaced vectors:

$$\bar{r}(L) = \frac{1}{8}\sum_{k=0}^{7} r\left(L\cos\theta_k, L\sin\theta_k\right) \quad (2)$$

where L is the distance (lag) at which the autocorrelation is computed and $\theta_k = (k-1)\pi/4$. In the experiments we used a set of six lags from 2px to 64px in octave spacing, this way obtaining six features per image.

B. Gabor filters

Gabor filters [22] decompose the information content of an image into different frequency and orientation channels. In the spatial domain the two-dimensional formulation of the filter is the following:

$$\psi(x,y) = \frac{F^2}{\pi\gamma\eta} e^{-F^2\left[\left(\frac{x'}{\gamma}\right)^2 + \left(\frac{y'}{\eta}\right)^2\right]} e^{i2\pi F x'}; \quad (3)$$

where x,y are the spatial coordinates and x',y' the coordinates after being rotated around the origin by an angle θ (Eq. 4).

$$\begin{cases} x' = x\cos(\theta) + y\sin(\theta) \\ y' = -x\sin(\theta) + y\cos(\theta) \end{cases} \quad (4)$$

In the experiments we used a bank of 24 filters (four frequencies and six orientations) with maximum frequency $F_M = 0.327\text{px}^{-1}$; the lower frequencies were obtained through octave down-spacing from F_M. The smoothing parameters η and γ were set respectively to = 1.1 and 0.8. We computed, as image features, the mean and standard deviation of the absolute value of each transformed image, therefore obtaining a feature vector of dimension $4 \times 6 \times 2 = 48$. Rotation-invariant features were obtained by taking, for each frequency, the absolute value of the discrete Fourier transform (DFT) over the six orientations (see [13] for details).

C. Grey-level co-occurrence matrices

Grey-level co-occurrence matrices encode the joint occurrence probability of the grey levels of pairs of pixels separated by a given displacement vector. The method was originally

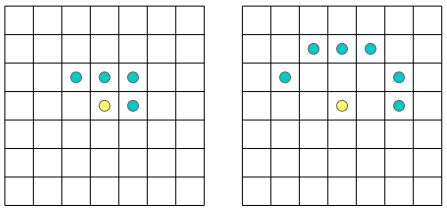

$R = 1$ $R = 2$

Fig. 3. Neighbourhood arrangement for GLCM features.

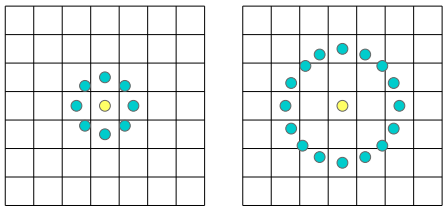

$m = 8, R = 1$ $m = 16, R = 2$

Fig. 4. Neighbourhood arrangement for LBP.

proposed by Haralick [11] more than forty years ago and has proved effective in many practical applications. In the experiments we considered sense–symmetric displacement vectors along digital circles of radii $R = 1$ and 2 as suggested in [2] (see Fig. 3).

From each co-occurrence matrix $\mathbf{M}$ we extracted the following five global statistical parameters:

Contrast:

$$\mathrm{CN} = \frac{1}{(G-1)^2} \sum_{u=0}^{G-1} \sum_{v=0}^{G-1} |u-v|^2 \mathbf{M}(u,v) \tag{5}$$

Correlation:

$$\mathrm{CR} = \frac{\sum_{u=0}^{G-1} \sum_{v=0}^{G-1} (u-\mu_u)(v-\mu_v)\mathbf{M}(u,v)}{2\sigma_u \sigma_v} + \frac{1}{2} \tag{6}$$

Energy:

$$\mathrm{EN} = \sum_{u=0}^{G-1} \sum_{v=0}^{G-1} \mathbf{M}(u,v)^2 \tag{7}$$

Entropy:

$$\mathrm{ET} = -\frac{1}{2\log_2(G)} \sum_{u=0}^{G-1} \sum_{v=0}^{G-1} \mathbf{M}(u,v) \log_2 [\mathbf{M}(u,v)] \tag{8}$$

Homogeneity:

$$\mathrm{HM} = \sum_{u=0}^{G-1} \sum_{v=0}^{G-1} \frac{\mathbf{M}(u,v)}{1+|u-v|} \tag{9}$$

where u, v represent the row- and column-wise coordinates along $\mathbf{M}$; μ_u, μ_v, σ_u and σ_v respectively the mean and standard deviation of the u-th (v-th) row (column) of $\mathbf{M}$. This way we obtained 4 × 5 = 20 features for $R = 1$ and 6 × 5 = 30 features for $R = 2$, therefore a total of 50 features. Rotation invariant features were computed by taking the absolute value of the DFT of the five features mentioned above – for further details see [2, Sec. 2.3].

D. Local binary patterns

Local binary patterns (LBP) [17] consider, as image features, the probability distribution of the binary patterns that can be generated from a neighbourhood of points when thresholded at a certain intensity value. The points are typically arranged into equally-spaced circular neighbourhoods (Fig. 4), and the grey-level of those not coinciding with image pixels are estimated through interpolation. In the literature this arrangement is usually referred to as (m, R), being m the number of points and R the radius (in pixels) of the circle.

The resulting binary patterns can be assigned a unique label in the following way:

$$\mathrm{LBP}_{m,R} = \sum_{i=0}^{m-1} 2^i \xi(I_i - I_c) \tag{10}$$

$$\xi(x) = \begin{cases} 1, & \text{if } x \geq 0 \\ 0, & \text{if } x < 0 \end{cases} \tag{11}$$

where I_c indicates the grey-level of the central point, I_i that of the i-th peripheral point starting from an arbitrary reference point $i = 0$, and $\xi(x)$ the thresholding function (Eq. 11). Rotation invariance is obtained by considering the probability distribution of the resulting *necklaces* – i.e. groups of binary patterns that can be transformed into one another by a rotation of multiples of $\pm 2\pi/m$ radians. The resulting rotation-invariant descriptor is referred to as $\mathrm{LBP}^{ri}_{m,R}$. In the experiments we used a concatenation of $\mathrm{LBP}^{ri}_{8,1}$ and $\mathrm{LBP}^{ri}_{16,2}$.

E. Granulometry

Digital granulometry is obtained by processing the input image through sets of morphological filters at different scales. In particular, by applying a set of openings (closings) at increasing scales L_i, $i \in \{1, \ldots, N\}$, we obtain a discrete approximation of the cumulative probability distribution of image structures brighter (darker) than their neighbourhoods. Mathematically, the approximated discrete granulometric curve $\mathcal{G}$ can be expressed as follows:

$$\mathcal{G}(L_i) = \frac{V_{L_i}(\mathbf{I}) - V(\mathbf{I})}{\Delta V_{L_N}(\mathbf{I})} \tag{12}$$

where $\mathbf{I}$ is the input image, $V(\mathbf{I})$ the sum of the grey-levels and $\Delta V_{L_N}(\mathbf{I})$ the global change resulting from opening the input image at the maximum scale L_N. From $\mathcal{G}(L_i)$ the probability size distribution (or pattern spectrum) is obtained through discrete differentiation – see also [3] for details. In the experiments we used a set of disc-shaped morphological

Table 1. Overall gender classification accuracy (in %) by image descriptor and imaging modality.

Classifier	Image descriptor	Epsilon			Proscope			Epsilon + Proscope		
		BH	FR	PL	BH	FR	PL	BH	FR	PL
1-NN	Autocorrelation	49.42	44.19	50.00	50.58	49.42	47.09	49.42	44.19	50.00
	Gabor filters	50.00	**61.05**	51.74	45.93	53.49	48.84	50.00	**61.05**	51.74
	GLCM	47.67	58.72	49.42	44.77	44.77	48.84	47.67	58.72	49.42
	Granulometry	51.74	54.07	44.77	51.16	51.74	51.16	51.74	54.07	44.77
	LBP	45.93	40.70	52.91	46.51	54.07	44.77	45.93	40.70	52.91
	Semi-variogram	52.33	51.16	51.74	52.33	47.67	52.33	52.33	51.16	51.74
SVM	Autocorrelation	48.26	52.33	49.42	51.16	**63.37**	55.23	49.42	51.74	52.33
	Gabor filters	43.60	53.49	53.49	53.49	58.72	57.56	43.02	54.65	53.49
	GLCM	53.49	53.49	53.49	53.49	53.49	52.91	53.49	53.49	53.49
	Granulometry	55.81	51.74	52.33	59.88	53.49	53.49	49.42	51.74	51.16
	LBP	45.35	52.91	53.49	43.60	51.16	55.23	50.00	56.98	51.74
	Semi-variogram	47.09	51.16	53.49	52.91	54.07	49.42	55.81	51.16	53.49

openings with radius from 2px to 64px in octave spacing (same setting used for autocorrelation – Sec. III-A).

F. Semi-variogram

The semi-variogram [10] is an averaged measure of the squared difference between the grey-levels of pairs of pixel set apart by a given displacement vector. Given δx and δy the components of the vector (also see Sec. III-A) the semi-variogram $\gamma(\delta x, \delta y)$ is given by:

$$\gamma(\delta x, \delta y) = \frac{1}{2WH} \sum_{w=1}^{W} \sum_{h=1}^{H} \left[\mathbf{I}\left(h + \delta x, w + \delta y\right) - \mathbf{I}\left(h, w\right)\right]^2 \tag{13}$$

To obtain rotation-invariant features we averaged the values over eight angularly equally-spaced vectors:

$$\bar{\gamma}(L) = \frac{1}{8} \sum_{k=0}^{7} \gamma\left(L\cos\theta_k, L\sin\theta_k\right) \tag{14}$$

where θ_k has the same meaning as in Sec. III-A. For a given set of lags L_i, $i \in \{1, \ldots, N\}$ the corresponding image features again are $f_i = \bar{\gamma}(L_i)$.

IV. Classification and data mapping

To test the gender discrimination capability of the texture skin features we ran a supervised image classification experiment using the image descriptors detailed in Sec. III. We considered both the features obtained from single-image modality (either Epsilon or Proscope separately) and a concatenation of them. We employed two different classification strategies: 1) nearest neighbourhood (1-NN) classifier with Euclidean distance (L_2) and support vector machines (SVM) with radial basis kernel.

Accuracy estimation was based on leave-one-out cross validation, i.e. for each given acquisition zone (either back of the hand, forearm or palm) all the four images of each subject in turn were simultaneously removed from the dataset and used for testing the classifier; the images of all remaining subjects were used for training. This procedure ensured that different images of the same subject could only appear either in the train or in the test set – but not in both at the same time, thus controlling for the effect of identity–specific information. SVM parameters (C and γ) were determined through 5-fold cross validation on the train set over the following grid of possible values: $C \in \{2^0, 2^2, \ldots, 2^8\}$ and $\gamma = \{2^{-8}, 2^{-6}, \ldots, 2^8\}$.

To further investigate the gender and identity information content of the features we applied dimensionality reduction through t-Distributed Stochastic Neighbour Embedding (t-SNE) [23]. This unsupervised mapping technique aims to find a non-linear correspondence between the high-dimensional feature space and a low-dimensional target space that models distances between pairs of points as well as possible, while preserving both the local and the global structure of the data. This is obtained by minimising the Kullback-Leibler divergence of transition probabilities between points in the two spaces.

V. Experimental results

The results of the gender classification experiments are summarised in Tab. 1. As can be seen, the estimated accuracy was invariably poor with all the feature combinations and classifiers used, and not very different from the accuracy of a random classifier (i.e. $\approx$50%).

Further, for each feature set/classifier combination in Tab. 1 we constructed the contingency table whose rows and columns respectively represent the true and the assigned gender. We then applied a 1-tailed Fisher's exact test to detect positive correlation between the true and assigned gender, under the null hypothesis that they are uncorrelated. After applying the Bonferroni correction, none of the results was found to be significant at a p-value of 10%, indicating that none of the combinations tested was significantly better than random classification.

It is worth noticing that, by contrast, consistently good performance was obtained when the same features were used for personal identification (43-class classification problem): in this case concatenation of Gabor features from Epsilon and Proscope images attained over 92% accuracy.

The above results are further confirmed by the unsupervised

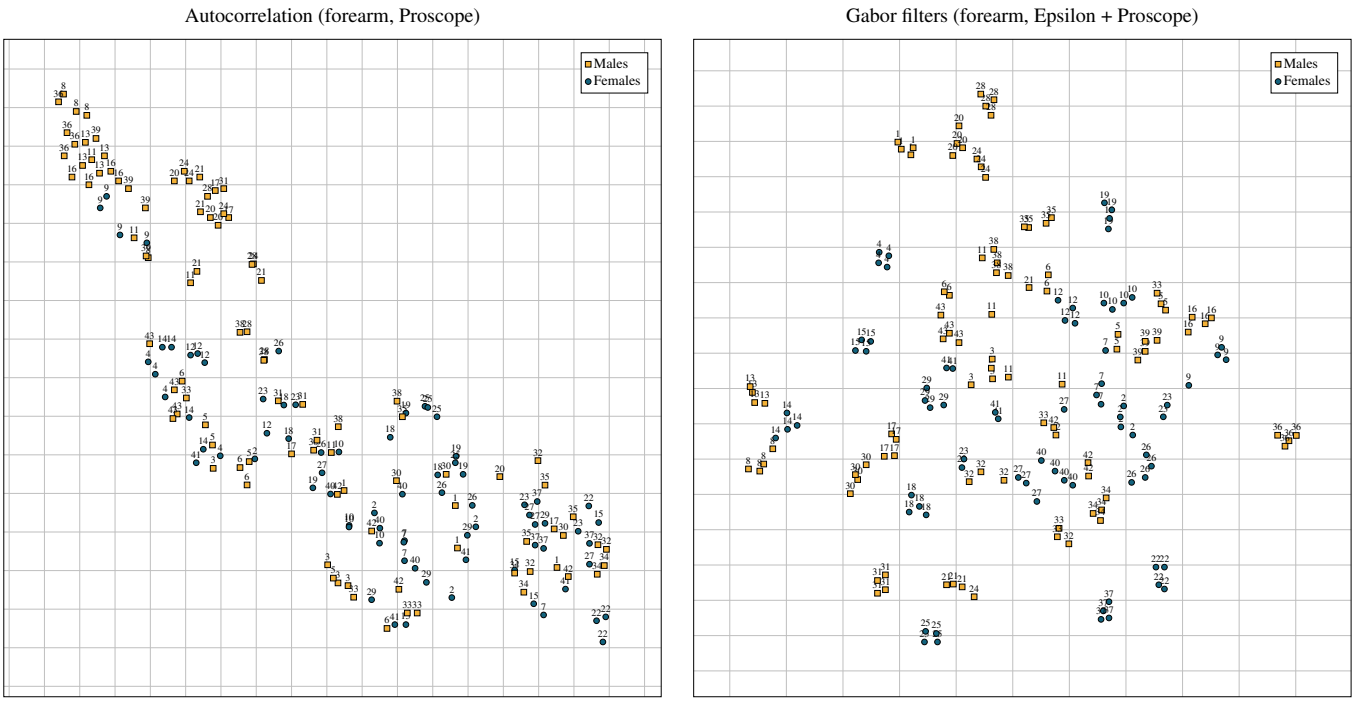

Fig. 5. Sample t-SNE maps showing the feature distribution in a two-dimensional space. Numbers indicate identities (there are four patterns for each individual).

approach shown in Fig 5. The two t-SNE maps depict the pattern distribution for the two best performing methods (Gabor features/forearm/Epsilon + Proscope and autocorrelation/forearm/Proscope). These plots confirm that whereas the individual identities are fairly obviously separable, gender does not appear to be.

VI. Discussion

Our experiments show that skin texture on the millimiter scale correlates very weakly with gender – if at all. Interestingly, a related analysis leading to different conclusions was recently reported by Xie et al. [25], where a database of skin textures from 80 persons was acquired using a custom rig featuring CCD camera at an approximately fixed distance from the skin and under controlled illumination conditions. The texture images thus obtained were similar to those produced by Proscope, but with a lower resolution ($\approx$ 450dpi). Image size was 288×384px; considering that Proscope images are 1600×1200px at $\approx$ 2822dpi in our system, that gives an imaging area of about 3.5cm^2 in [25] as opposed to about 1cm^2 after trimming in our experiments, which is still comparable. Likewise, features used in [25] were a sparse representation based on MR8 filters [24] – closely related to Gabor filters, which we also used in our tests. In spite of the similarities in acquisition and processing, however, [25] reports a gender classification accuracy of 98.60% based on the texture of the back of the hand, where our best result was 63% – dramatically lower and not statistically significant.

Crucially, in [25] samples collected from *the same individuals*, albeit in two different sessions, were used both for training and testing the gender classifier. This is in actual fact *a relaxation of the personal identification problem*, therefore not a good benchmark for gender recognition performance as it does not control for identity–specific information. To see this consider that, as we have shown in Fig. 5 and Section V, skin texture is very distinctive of identity. Indeed personal identification accuracies of around 90% are reported in [25] based on very the same features used for gender discrimination (we obtained a quite comparable 92% for identification on our data). Using the same identities for training and testing therefore amounts to performing identification while condoning all instances in which a person is mistaken for another person of the same sex.

The observation in [25] that female and male subjects have different skin texture patterns on the back of their hand, with the female texture being "much finer" (as exemplified by Fig. 5 in [25]) should be considered with care in the light of our results and may not generalise to other datasets (see Fig. 6 in our work).

Finally, it must be noted that both our analysis and the one in [25] focus entirely on skin texture. While the existence of physiological differences in skin related to gender is well established [8], these do not seem to affect texture enough for reliable gender identification. Population differences between the genders in the distribution of skin tone [12] and thickness and water retention capability [21] have been documented, but for specific individuals and one-shot acquisitions these are likely to be obscured by inter-personal and time variability.

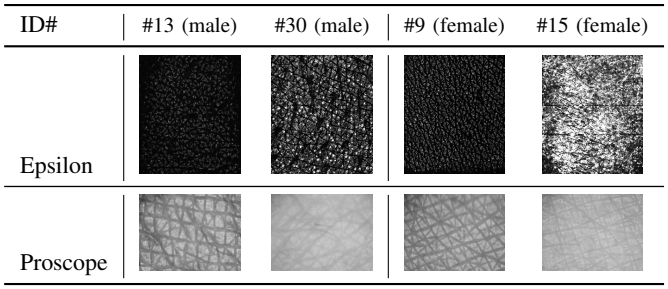

Fig. 6. Inter–personal variability in the skin texture of the back of the hand (including perceived coarseness) overshadows gender differences.

VII. Conclusions

In spite of the common assumption that male and female skins have a distinctly different appearance, the question of whether skin texture allows discriminating between genders has seldom been addressed quantitatively. We investigated this issue using two different imaging modalities (visual and capacitive), a varied array of image features, two supervised classification strategies (1-NN and SVM) and a state-of-the-art unsupervised approach (t-SNE). Our database included subjects of different age and ethnicity, and we acquired skin texture from three different areas. Statistical analysis of the results using Fisher's exact test shows no evidence that skin texture can be used for gender discrimination, individual variations swamping whatever weak correlation there may be. This contradicts both common wisdom and, notably, the results of a previous study [25]. Admittedly, our investigation is far from exhaustive from the point of view of age, ethnicity and the particular (Western) culture in which the subjects are immersed, which may affect skin care and thus skin appearance. It could also be argued that microtexture does not exhaust skin information (and indeed, in the case of face biometrics gender information is carried by different image frequencies than used for identification). However, our experiments clearly show that any naive assumption on visual differences between the male and female skin should be avoided, and cast serious doubts on whether skin texture is useful for gender discrimination.

Acknowldegements

This work was partially supported by the Dept. of Engineering at the University of Perugia, Italy (UniPG Eng) under grants '*BioMeTron* – Fundamental research D.D. 20/2015' and 'MOND15FB'. F. S. performed part of this work as a Visiting Researcher at UniPG Eng. He gratefully acknowledges the support of UniPG under international mobility grant 'D.R. n.2270/2015' and a Centre for Intelligent Sensing travel grant.

References

[1] C. D. Barclay, J. E. Cutting, and L. T. Kozlowski. Temporal and spatial factors in gait perception that influence gender recognition. *Perception & psychophysics*, 23(2):145–152, 1978.

[2] F. Bianconi and A. Fernández. Rotation invariant co-occurrence features based on digital circles and discrete Fourier transform. *Pattern Recognition Letters*, 48:34–41, 2014.

[3] F. Bianconi, F. Di Maria, C. Micale, A. Fernández, and R. Harvey. Grain-size assessment of fine and coarse aggregates through bipolar area morphology. *Machine Vision and Applications*, 26(6):775–789, 2015.

[4] Biox Systems Ltd. Epsilon model E100 product description, 2016. Available online at `http://www.biox.biz/Products/Epsilon/E100ProductDescription.php`. Last accessed on Sep. 11, 2016.

[5] Bodelin Technologies. Proscope HR specifications, 2015. Available online `https://www.bodelin.com/files/proscope/docs/ProScopeHR2_Specifications.pdf`. Last accessed on November 26, 2015.

[6] V. Bruce, A. M. Burton, E. Hanna, P. Healey, O. Mason, A. Coombes, R. Fright, and A. Linney. Sex discrimination: how do we tell the difference between male and female faces? *Perception*, 1993.

[7] J. A. Cattarin, J. K. Thompson, C. Thomas, and R. Williams. Body image, mood, and televised images of attractiveness: The role of social comparison. *Journal of Social and Clinical Psychology*, 19(2):220–239, 2000.

[8] P. U. Giacomoni, T. Mammone, and M. Teri. Gender-linked differences in human skin. *Journal of dermatological science*, 55(3):144–149, 2009.

[9] E. N. Glenn. Yearning for lightness: Transnational circuits in the marketing and consumption of skin lighteners. *Gender & society*, 2008.

[10] A. Hanbury, U. Kandaswamy, and D. A. Adjeroh. Illumination-invariant morphological texture classification. In *Mathematical Morphology: 40 years on. Proceedings of the 7th International Symposium on Mathematical Morphology*, volume 30 of *Computational Imaging and Vision*, pages 377–386, April 2005.

[11] R. M. Haralick, K. Shanmugam, and I. Dinstein. Textural features for image classification. *IEEE Transactions on Systems, Man, and Cybernetics*, 3(6):610–621, 1973.

[12] A. Kalla and S. Tiwari. Sex differences in skin colour in man. *Acta geneticae medicae et gemellologiae*, 19(03):472–476, 1970.

[13] F. Lahajnar and S. Kovacic. Rotation-invariant texture classification. *Pattern Recognition Letters*, 24(9-10):1151–1161, 2003.

[14] X. Li, S. J. Maybank, S. Yan, D. Tao, and D. Xu. Gait components and their application to gender recognition. *Systems, Man, and Cybernetics, Part C: Applications and Reviews, IEEE Transactions on*, 38(2):145–155, 2008.

[15] E. Mäkinen and R. Raisamo. Evaluation of gender classification methods with automatically detected and aligned faces. *Pattern Analysis and Machine Intelligence, IEEE Transactions on*, 30(3):541–547, 2008.

[16] Office for National Statistics. Harmonised concepts and questions for social data sources. primary principles. version 3.3, 2015. Available online `http://www.ons.gov.uk/ons/guide-method/harmonisation/primary-set-of-harmonised-concepts-and-questions/ethnic-group.pdf`. Last accessed on November 26, 2015.

[17] T. Ojala, M. Pietikäinen, and T. Mäenpää. Multiresolution gray-scale and rotation invariant texture classification with local binary patterns. *IEEE Transactions on Pattern Analysis and Machine Intelligence*, 24(7):971–987, 2002.

[18] X. Ou, W. Pan, and P. Xiao. In vivo skin capacitive imaging analysis by using grey level co-occurrence matrix (GLCM). *International Journal of Pharmaceutics*, 460(1-2):28–32, 2014.

[19] D. Rubin. A simple autocorrelation algorithm for determining grain size from digital images of sediment. *Journal of Sedimentary Research*, 74(1):160–165, 2004.

[20] C. Shan. Learning local binary patterns for gender classification on real-world face images. *Pattern Recognition Letters*, 33(4):431–437, 2012.

[21] S. Shuster, M. M. Black, and E. Mcvitie. The influence of age and sex on skin thickness, skin collagen and density. *British Journal of Dermatology*, 93(6):639–643, 1975.

[22] M. Turner. Texture discrimination by Gabor functions. *Biological Cybernetics*, 55(2-3):71–82, 1986.

[23] L. Van der Maaten and G. Hinton. Visualizing data using t-sne. *Journal of Machine Learning Research*, 9(2579-2605):85, 2008.

[24] M. Varma and A. Zisserman. A statistical approach to texture classification from single images. *International Journal of Computer Vision*, 62(1-2):61–81, 2005.

[25] J. Xie, L. Zhang, J. You, D. Zhang, and X. Qu. A study of hand back skin texture patterns for personal identification and gender classification. *Sensors*, 12(7):8691–8709, 2012.

[26] J.-H. Yoo, D. Hwang, and M. S. Nixon. Gender classification in human gait using support vector machine. In *Advanced concepts for intelligent vision systems*, pages 138–145. Springer, 2005.